Available online at www.sciencedirect.com
SCIENCE DIRECT
Geochimica et Cosmochimica Acta 70 (2006) 1655–1667
Geochimica
www.elsevier.com/locate/gca

Does reactive surface area depend on grain size? Results from pH 3, 25 °C far-from-equilibrium flow-through dissolution experiments on anorthite and biotite

Mark E. Hodson *

Department of Soil Science, School of Human and Environmental Sciences, University of Reading, Whiteknights, Reading, Berkshire, RG6 6DW, UK

Received 25 July 2005; accepted in revised form 4 January 2006

Abstract

Laboratory determined mineral weathering rates need to be normalised to allow their extrapolation to natural systems. The principle normalisation terms used in the literature are mass, and geometric- and BET specific surface area (SSA). The purpose of this study was to determine how dissolution rates normalised to these terms vary with grain size. Different size fractions of anorthite and biotite ranging from 180–150 to 20–10 μm were dissolved in pH 3, HCl at 25 °C in flow through reactors under far from equilibrium conditions. Steady state dissolution rates after 5376 h (anorthite) and 4992 h (biotite) were calculated from Si concentrations and were normalised to initial- and final- mass and geometric-, geometric edge- (biotite), and BET SSA. For anorthite, rates normalised to initial- and final-BET SSA ranged from 0.33 to 2.77×10^{-10} $mol_{feldspar}\ m^{-2}\ s^{-1}$, rates normalised to initial- and final-geometric SSA ranged from 5.74 to 8.88×10^{-10} $mol_{feldspar}\ m^{-2}\ s^{-1}$ and rates normalised to initial- and final-mass ranged from 0.11 to 1.65 $mol_{feldspar}\ g^{-1}\ s^{-1}$. For biotite, rates normalised to initial- and final-BET SSA ranged from 1.02 to 2.03×10^{-12} $mol_{biotite}\ m^{-2}\ s^{-1}$, rates normalised to initial- and final-geometric SSA ranged from 3.26 to 16.21×10^{-12} $mol_{biotite}\ m^{-2}\ s^{-1}$, rates normalised to initial- and final-geometric edge SSA ranged from 59.46 to 111.32×10^{-12} $mol_{biotite}\ m^{-2}\ s^{-1}$ and rates normalised to initial- and final-mass ranged from 0.81 to 6.93×10^{-12} $mol_{biotite}\ g^{-1}\ s^{-1}$. For all normalising terms rates varied significantly ($p \leqslant 0.05$) with grain size. The normalising terms which gave least variation in dissolution rate between grain sizes for anorthite were initial BET SSA and initial- and final-geometric SSA. This is consistent with: (1) dissolution being dominated by the slower dissolving but area dominant non-etched surfaces of the grains and, (2) the walls of etch pits and other dissolution features being relatively unreactive. These steady state normalised dissolution rates are likely to be constant with time. Normalisation to final BET SSA did not give constant ratios across grain size due to a non-uniform distribution of dissolution features. After dissolution coarser grains had a greater density of dissolution features with BET-measurable but unreactive wall surface area than the finer grains. The normalising term which gave the least variation in dissolution rates between grain sizes for biotite was initial BET SSA. Initial- and final-geometric edge SSA and final BET SSA gave the next least varied rates. The basal surfaces dissolved sufficiently rapidly to influence bulk dissolution rate and prevent geometric edge SSA normalised dissolution rates showing the least variation. Simple modelling indicated that biotite grain edges dissolved 71–132 times faster than basal surfaces. In this experiment, initial BET SSA best integrated the different areas and reactivities of the edge and basal surfaces of biotite. Steady state dissolution rates are likely to vary with time as dissolution alters the ratio of edge to basal surface area. Therefore they would be more properly termed pseudo-steady state rates, only appearing constant because the time period over which they were measured (1512 h) was less than the time period over which they would change significantly.

1. Introduction

Mineral weathering plays a crucial role in a variety of important ecosystem processes such as the release of plant nutrients in soil (Marschner, 1995), the neutralisation of acid rain (Nilsson and Grennfelt, 1988) and regulation of

* Fax: +44 0 181 931 6660.
E-mail address: m.e.hodson@reading.ac.uk.

0016-7037/$ - see front matter © 2006 Elsevier Inc. All rights reserved.
doi:10.1016/j.gca.2006.01.001

atmospheric CO_2 (Berner, 1995). The importance of mineral dissolution is testified to by: (a) the large number of laboratory experiments in which minerals are dissolved in an attempt to determine universally applicable dissolution rate equations and, (b) field studies performed in order to relate what happens in nature to what happens in the laboratory (e.g. White and Brantley, 1995; Brantley, 2004; White, 2004 and references therein). Whilst much progress has been made in understanding both macroscopic and microscopic controls on dissolution many fundamental problems remain. The problem that this paper is concerned with is the normalising term for mineral dissolution rates.

In order to apply laboratory determined mineral dissolution rates to the field they have to be normalised. The majority of dissolution studies normalise dissolution rates to either mass or surface area of mineral. Surface area is normally measured as specific surface area (SSA) i.e., surface area per unit mass ($m^2\,g^{-1}$) and then multiplied by a mass term to give total surface area available for dissolution. Specific surface area terms used are either geometric, calculated by assuming that the mineral particles under consideration have smooth surfaces and a regular, uniform geometry or BET, calculated using N_2 (or less commonly Kr or Ar) adsorption and the BET isotherm (Brunauer et al., 1938; Gregg and Sing, 1982).

Briefly, the problems with these normalising terms are as follows. Mass does not scale linearly with surface area so that if particles dissolve over their entire surface or at specific sites on their surface, mass normalised dissolution rates will be different for particles of different grain size (and mass). Typically, mineral particles do not have regular geometric shapes or smooth surfaces so use of geometric surface area terms introduces errors into any normalisation. Neither geometric nor BET surface area discriminates between areas of sample surface which have differing reactivities. Thus, the use of a bulk surface area normalising term assumes that on average over the entire range of different types of surface with differing reactivities this term scales to reactive surface area. A fuller discussion of the relative merits of normalisation to geometric and BET SSA is given by Wolff-Boenisch et al. (2004).

Etch pits and other surface depressions have been observed in many scanning electron microscope (SEM), atomic force microscope (AFM) and interferometric studies to form on many different minerals during dissolution and indicate the existence of areas of differing reactivities on mineral surfaces (e.g., Wilson, 1975; Grandstaff, 1978; Berner et al., 1980; Brantley et al., 1986; Zhang et al., 1993; Lee and Parsons, 1995; Lee et al., 1998; Lütgge et al., 1999; Rufe and Hochella, 1999; Gautier et al., 2001; Arvidson et al., 2004; Hu et al., 2005; Vinson and Lüttge, 2005). Much progress has been made in characterising the relative dissolution rates of different crystallographic faces and different sites on grain surfaces through the use of AFM, interferometry and X-ray reflectivity (e.g., Gratz et al., 1990; Lee et al., 1998; Lütgge et al., 1999; Rufe and Hochella, 1999; Bosbach et al., 2000; Fenter et al., 2003; Arvidson et al., 2004; Vinson and Lüttge, 2005). For quartz and feldspar it has been shown (Lee et al., 1998; Lütgge et al., 1999; Gautier et al., 2001) that in far from equilibrium laboratory studies the dissolution rate of etch pits can be up to several orders of magnitude greater than the surrounding non-etch pit surface. However, Lee et al. (1998) and Gautier et al. (2001) concluded that because the area of etch pits is far less than the remaining surface of mineral grains, dissolution rates measured in laboratory studies are dominated by the non-etch pit surface.

Holdren and Speyer (1985, 1987) reported a lack of constancy for the BET surface area normalised dissolution rates of different grain-sized feldspar powders and attributed this to the relative spacing of reactive sites and grain size. However, dissolution of the different size fractions was performed at different solution Al concentrations and the different rates are most likely due to aqueous solution composition effects (Oelkers et al., 1994; Oelkers, 2001). Stillings and Brantley (1995) dissolved microcline, albite, oligoclase, labradorite, and bytownite at pH 3. Dissolution of the first four of these feldspars generated surface topography due to preferential dissolution at reactive sites whilst the bytownite showed little evidence of selective dissolution. Initial and final BET SSA were measured on the powders and a "current" BET SSA calculated assuming a constant, linear rate of change in BET SSA over the duration of the experiment. Dissolution rates were only constant when normalised to "current" rather than initial or final BET SSA. More recently, and in contrast to the results of Stillings and Brantley (1995), Gautier et al. (2001) determined that geometric SSA normalised dissolution rates gave constant values for quartz dissolution over time whilst BET SSA normalised rates decreased. Quartz dissolution generated etch pits which caused an increase in BET but not geometric SSA. Gautier et al. (2001) concluded that the walls of the etch pits were unreactive so that whilst BET surface area increased during dissolution, reactive surface area did not. Although the floors of the etch pits dissolved more rapidly than the non-etched surface the small areal extent of the etch pit floors meant that the bulk dissolution of the quartz was dominated by the non-etch surface. Several studies suggest that sheet silicate dissolution occurs from the edges of mineral grains rather than occurring over the entire mineral surface (Ross, 1969; Knuass and Wolery, 1989; Acker and Bricker, 1992; Turpault and Trotignon, 1994; Kalinowski and Schweda, 1996; Rufe and Hochella, 1999; Bosbach et al., 2000; Köhler et al., 2005). Acker and Bricker (1992) reported that at pH 3 for biotite of grain size <149, 149–420, and >420 μm, mass normalised dissolution rates increased with decreasing grain size whereas BET SSA normalised dissolution rates decreased with grain size. Turpault and Trotignon (1994) showed a good correlation between Mg release from biotite and edge surface area (termed lateral surface area in their work) and determined that the edges of biotite dissolved at 30–300 times the rate of the basal surfaces. More recently Köhler et al. (2005) dissolved illite and suggested on the basis of their results and other studies in the literature that sheet silicate dissolution

rates should never reach a steady state due to dissolution being dominated by grain edges and the ratio of edge to total surface area varying over time.

The aim of the experiments reported in this paper was to determine the most appropriate rate normalisation term for normalising anorthite and biotite dissolution in the laboratory, i.e., a normalisation term that results in constant dissolution rates for different grain sizes. This was achieved by dissolving mineral powders of different grain size in undersaturated, pH 3, HCl, 25 °C conditions and comparing steady state dissolution rates normalised to a variety of terms. The hypothesis being tested was that different grain sizes of the same mineral should dissolve at the same rate. Therefore, an appropriate dissolution rate normalising term should give constant dissolution rates over a range of grain sizes. New dissolution experiments were performed rather than literature data being used in order to obtain an internally consistent data set. Dissolution rates were normalised to initial- and final- mass and geometric-, geometric edge- (for biotite), and BET- specific surface area.

2. Materials and methods

Grass Valley anorthite and a biotite from Bancroft, Ontario (both obtained from Wards Scientific) were ground, sieved to give different size fractions (ranging from 180–150 to 20–10 μm), ultrasonically cleaned in deionised water, air dried, and then purified by magnetic separation using a Franz magnetic separator. Mineral bulk composition was determined using X-ray fluorescence and recalculated to a mineral formula following the methods of Deer et al. (1992). Compositions were $Na_{0.1}Ca_{1.1}Al_{1.9}Si_{2.0}O_8$ (i.e., An92) for anorthite and $K_{1.7}Mg_{3.5}Fe_{2.4}Al_{1.8}Ti_{0.2}\ Si_{6.0}O_{20}(OH)_4$ for biotite (assuming all Fe was present as Fe^{2+}).

Specific surface areas of the samples used in the study are given in Tables 1 (anorthite) and 2 (biotite). Initial geometric SSA was calculated assuming that the anorthite particles were cubes and the biotite particles cuboids (Fig. 1). Mean particle length for anorthite grains was assumed to lie at the mid-point between the maximum and minimum mesh size of the sieves used to separate the different grain size fractions. These dimensions were also assumed for the *a* and *b* lengths of the biotite particles; the *c* length was estimated from observations using a Philips XL-30 Field emission scanning electron microscope. The geometric SSA of the biotite edges (i.e., surface area associated with sides *ac* and *bc* expressed on a per mass basis, $m^2\ g^{-1}$) was also calculated and is referred to below as geometric edge SSA. Initial BET SSA of the different size fractions was determined using nitrogen adsorption and application of the BET isotherm (Brunauer et al., 1938; Gregg and Sing, 1982).

Masses of sample used in the dissolution experiments were selected to give the same initial surface area of mineral for each grain size calculated on the basis of initial BET SSA. For the anorthite, each reactor contained initially ca. 0.15 m^2 powder, for the biotite ca. 1.25 m^2 powder except for the second 53–20 μm experiment where shortage of powder resulted in only 1.00 m^2 of surface area being present. Far from equilibrium dissolution experiments were carried out using pH 3, HCl in continuous flow reactors comprising 125 mL polypropylene reaction vessels each containing 110 mL HCl, a TFE (55) coated Nalgene floating stir bar and a mineral powder. Reaction vessels were placed on a heated magnetic stir plate set to 25 °C.

Table 1
Mass, geometric SSA, and BET SSA of anorthite before and after dissolution

	Grain size (μm)				
	180–150	105–90	75–63	53–20	20–10
Mass/g					
Initial	1.79	1.49	1.28	0.66	0.30
Final	1.61	1.32	1.10	0.46	0.16
	1.62	1.31	1.10	0.48	—
Geometric specific surface area ($m^2\ g^{-1}$)					
Initial	0.013	0.023	0.033	0.062	0.151
Final	0.014	0.024	0.034	0.070	0.187
	0.014	0.024	0.034	0.069	—
BET specific surface area ($m^2\ g^{-1}$)					
Initial	0.08	0.10	0.12	0.23	0.42
Final	0.38	0.49	0.50	0.69	0.60

Where two values are given these are for replicate experiments. Initial mass of material used in the experiments, geometric SSA and BET SSA were the same between replicates. Single values for final BET SSA are given as replicate samples were combined to give sufficient powder for a BET measurement to be performed. Geometric SSA calculated assuming a density of 2.65 g cm^{-3}.

Table 2
Mass, geometric SSA, geometric edge SSA, and BET SSA of biotite before and after dissolution

	Grain size (μm)				
	180–150	105–90	75–63	53–20	20–10
Mass/g					
Initial	2.19	1.88	1.37	0.86	0.27
	2.19	—	—	0.69	0.27
Final	2.16	1.85	1.34	0.83	0.24
	2.16	—	—	0.66	0.24
Grain thickness on basis of SEM observations (μm)	5	4	2	2	2
Geometric specific surface area ($m^2\ g^{-1}$)					
Initial	0.141	0.180	0.353	0.370	0.422
Final (constant *c* dimension, see Fig. 1)	0.180	0.353	0.371	0.428	
	0.141	—	—	0.371	0.428
Geometric edge specific surface area ($m^2\ g^{-1}$)					
Initial	0.008	0.014	0.019	0.037	0.089
Final (constant *c* dimension, see Fig. 1)	0.008	0.014	0.020	0.037	0.094
	0.008	—	—	0.037	0.094
BET specific surface area ($m^2\ g^{-1}$)					
Initial	0.56	0.66	0.92	1.44	4.74
Final	0.58	0.83	1.15	1.80	4.43
	0.75			1.65	3.42

Where two values are given these are for replicate experiments. Initial geometric SSA, geometric edge SSA, BET SSA, and grain thickness were the same between replicates. Geometric SSA calculated assuming a density of 3.00 g cm^{-3}.

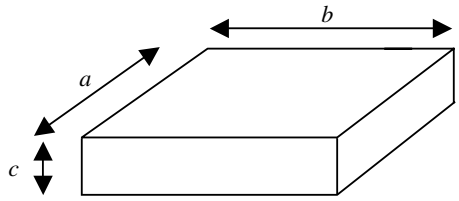

Fig. 1. Dimensions of biotite particles.

The HCl was pumped from polypropylene bottles kept in a heated water bath set at 25 °C. Flow rates were $4.7 \pm 0.3 \times 10^{-4}$ mL s^{-1} (1.7 ± 0.1 mL h^{-1}) giving a fluid residence time in the reactors of ca. 65 h. Experiments were carried out in duplicate except for the 20–10 μm anorthite, 105–90 μm biotite and 75–63 μm biotite experiments due to paucity of powder. The chemistry of the output solutions was monitored, initially every 24 h but by the end of the experiments at longer intervals (Table 3, Appendices A and B). Solutions were analysed for Al, Ca, and Si (anorthite) and Al, Fe, K, Mg, and Si (biotite) using inductively coupled plasma-atomic emission spectroscopy (ICP-AES). pH was measured for the last five output solutions. Solution compositions were analysed using PHREEQC (Parkhurst and Appelo, 1999) to determine whether they were saturated with respect to any phases. At the end of the experiment powders were retrieved from the reaction vessels, washed thoroughly in deionised water, dried overnight at 30 °C and their BET SSA determined (Tables 1 and 2). Anorthite samples were bulked in order to obtain sufficient sample for an accurate BET measurement.

Table 3
Si concentrations from dissolution experiments used to calculate dissolution rates

Grain size (μm)	Si concentration (μg L^{-1}) Time (h)					Average ± SD
	3576	3840	4056	4872	5376	
Anorthite						
180–150	*2823*	*3826*	*3908*	*2777*	*2460*	*3159 ± 662*
	2462	2548	2641	2820	2706	2635 ± 139
105–90	3202	2960	3043	2835	—	3010 ± 154
	2662	*2381*	*2391*	*3566*	*2759*	*2752 ± 484*
75–63	3331	3101	3102	3044	3066	3129 ± 116
	3476	3082	3173	3082	2773	3117 ± 252
53–20	3371	3289	3209	3311	3165	3269 ± 82
	3515	3225	3165	2937	2685	3106 ± 312
20–10	3405	3407	3233	2786	3685	3303 ± 331
	Time (h)					
	3480	4008	4320	4728	4992	
Biotite						
180–150	651	680	671	670	802	695 ± 61
	545	650	659	625	652	626 ± 47
105–90	516	540	591	560	661	574 ± 56
75–63	523	585	541	545	604	560 ± 34
53–20	624	688	809	716	790	726 ± 75
	538	585	618	570	671	597 ± 51
20–10	581	570	574	550	596	574 ± 17
	599	616	584	554	649	600 ± 36

Where two lines of data are given these are for replicate experiments. N.B. for the anorthite 20–10 μm fraction time intervals are 3048, 3264. 4080, 4584, and 5568 h. Data in italics have SD > 10% of the mean and are not included in further analysis.

Final mass of material in the experiments (Tables 1 and 2) was calculated in the same way as Gautier et al. (2001) by calculating the mass of material remaining in the reactors at each sampling event on the basis of Si concentration in the output solution from the flow through reactors and mineral composition.

$$M_T = M_{T-1} - \left[\frac{\Delta[\mathrm{Si}] \times q \times \Delta t \times m_{\min}}{10^6 \times m_{\mathrm{Si}} \times n}\right], \quad (1)$$

where M_T is the mass of mineral in reactor at time of output solution sampling event T (g); M_{T-1} is the mass of mineral in reactor at time of output solution sampling event $T-1$ (g); Δ [Si] is the change in concentration of Si between input and output solution (mg L^{-1}); q is the flow rate (mL s^{-1}); Δt is the time since last sampling event (s); $m_{\min}$ is the formula weight of dissolving mineral; m_{Si} is the atomic weight of Si; and n is the stoichiometric coefficient of Si in the formula unit of the dissolving mineral.

Final geometric SSA (and final geometric edge SSA for biotite) (Tables 1 and 2) was calculated by assuming that dissolution resulted in a reduction in grain size. The reduction in particle dimensions that would account for the calculated mass reduction obtained from Eq. (1) was determined. These dimensions were used to calculate the geometric SSAs. An equal reduction in the length of all sides of the anorthite cubes was assumed. No change in thickness of the biotite particles was observable by SEM after dissolution so a constant c dimension and an equal reduction in the a and b dimensions (Fig. 1) was assumed.

Dissolution rates for the different size fractions were calculated using the formula:

$$R_{\mathrm{Si}} = \frac{q \times \Delta[\mathrm{Si}]}{10^6 \times \mathrm{SSA} \times M \times m_{\mathrm{Si}} \times n}, \quad (2)$$

where R_{Si} is the dissolution rate calculated from release of Si ($\mathrm{mol}_{\mathrm{mineral}}$ $\mathrm{m}^{-2}{}_{\mathrm{mineral}}$ s^{-1}); SSA is the specific surface area (initial- or final- geometric, edge or BET SSA) (m^2 g^{-1}); and M is the initial- or final- mass of mineral present in reactor (g).

For mass normalised dissolution rates the SSA term was left out of Eq. (2). Calculations were performed using "current" mass and SSA as well as the initial- and final-mass and SSA terms. Current mass was determined using Eq. (1) and current geometric SSA terms were calculated for appropriate grain size reductions that would result in the calculated mass reduction. Current BET SSA was calculated by assuming that changes in BET SSA were linear with time between the initial and final values. Steady state rates were practically identical to those calculated using final values and are therefore not reported. Dissolution rates were calculated using Al and Ca data (anorthite) and Al, Fe, K, and Mg data (biotite) in addition to the Si data but results gave the same trends and led to the same conclusions so are not reported here.

Statistical analysis of data was performed using the statistics package SigmaStat3 (SPSS, 2003). Dissolution rates derived using the Si data reported in Table 3 for pairs of the same-sized mineral grains were normally distributed and were compared with *t* tests. Variation in calculated dissolution rates between different grain sizes was determined using analysis of variance (ANOVA) for normally distributed data (using both the Holm–Sidak and Tukey test) or Kruskal–Wallis one way analysis of variance on ranks for data that was either not normally distributed or which had unequal variances.

3. Results and discussion

3.1. Solution composition

Solution compositions are given in Appendix A (anorthite) and Appendix B (biotite). At the end of the experiments the standard deviation about the mean of solution Si concentrations determined for the last five sampling events (1800 h, anorthite; 1512 h, biotite) was $\leqslant$10% for the majority of reactors (Table 3). Analysed solution compositions for the anorthite data showed more scatter than for the biotite. Uncertainty in the determined concentration of Si is approximately 10%. Experiments where the standard deviation about the mean Si concentration for the last five sampling events was $\leqslant$10% were therefore assumed to have reached steady state and solution concentrations were used to calculate dissolution rates. Experiments where the standard deviation of Si concentration was >10% of the mean were not included in further analysis.

No secondary phases were observed during extensive SEM investigation of the mineral grains after dissolution. Calculations using PHREEQC indicated that all of the solutions were under-saturated with respect to potentially precipitating phases. Additionally, all the solutions had approximately the same level of undersaturation. Therefore in the following it is assumed that any differences between dissolution rates are not a function of affinity effects.

3.2. Changes in specific surface area

As dissolution proceeded SSA for both the anorthite and biotite grains increased although in some cases the increase was negligible (Tables 1 and 2). Increases in SSA are to be expected as dissolution proceeds. For geometric calculations where dissolution is assumed to cause a reduction in grain size smaller particles have a larger surface area to mass ratio than larger particles. BET SSA will also increase for the same reason if dissolution is manifest by a reduction in grain size. For the anorthite, dissolution generated both etch pits and dissolution cracks (Figs. 2a and b). This generates additional surface area as mass is lost so again, the surface area to mass ratio of the particles increases. The exception to the increase in SSA was for BET SSA of the 20–10 μm biotite fraction. The reason for the decrease is not clear.

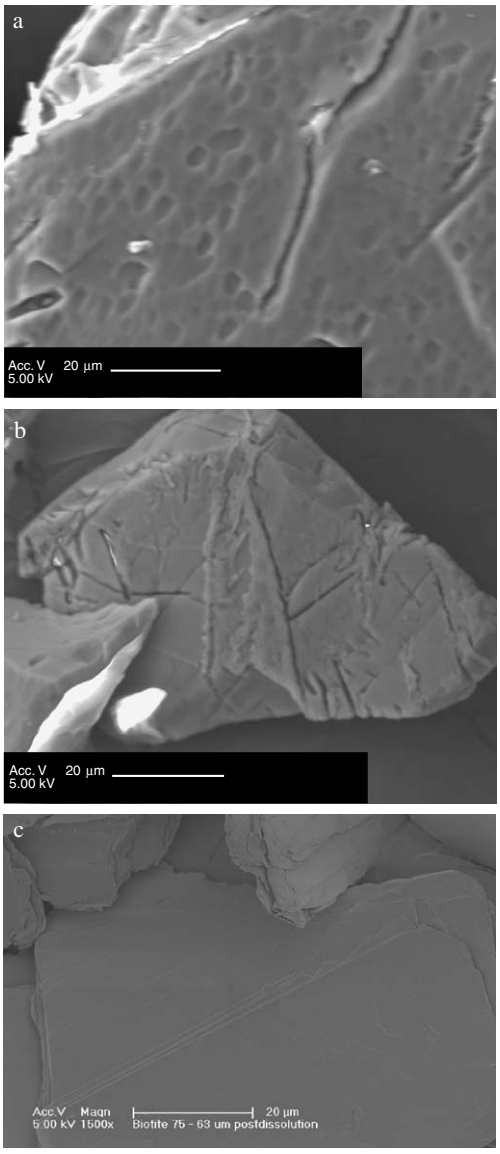

Fig. 2. SEM Secondary electron images of (a) 180–150 μm size anorthite particle after dissolution showing etch pit formation, (b) 75–63 μm size anorthite particle after dissolution showing many cracks running across grain surface, (c) 75–63 μm size biotite particle after dissolution showing smooth surface. Etch pit distribution between grains of anorthite was highly variable, ranging from 0 to 2.2×10^6 pits cm^{-2}. Average pit density was 3.7×10^5 pits cm^{-2}, average pit spacing 16 μm and average pit diameter 3 ± 1 μm.

3.3. Dissolution rates

Dissolution rates were calculated using solution data for all sampling times over the duration of the experiment. Rates were normalised to initial- and final-mass, and BET, geometric and geometric edge (biotite) SSA. For all normalising terms used, dissolution rate showed the characteristic initial rapid decrease in rate with time followed by a levelling off to a steady state rate. The solution data used to calculate the steady state dissolution rates are given in Table 3. Calculated steady state dissolution rates are given in Tables 4 (anorthite) and 5 (biotite). Regardless of the normalisation method dissolution rates obtained for pairs

Table 4
Mean dissolution rates for anorthite calculated from Si data in Table 3 and using initial- and final- BET SSA (BET), geometric SSA (Geometric) or mass (Mass) as the rate normalising term (10^{-10} $mol_{feldspar}$ m^{-2} s^{-1})

Grain size (μm)	Normalising term					
	Initial			Final		
	BET	Geometric	Mass	BET	Geometric	Mass
180–150	1.36	8.31	0.11	0.33	8.88	0.13
105–90	1.55	6.72	0.16	0.36	7.28	0.18
75–63	1.61	5.77	0.19	0.44	6.37	0.22
	1.61	5.75	0.19	0.44	6.35	0.22
53–20	1.67	6.17	0.38	0.79	7.83	0.55
	1.58	5.86	0.36	0.73	7.29	0.50
20–10	2.03	5.74	0.86	2.77	8.79	1.65
Average	1.63	6.32	0.32	0.84	7.54	0.49
SD (%)	12	15	80	104	14	109

Where two values are given these are for replicate experiments.

Table 5
Mean dissolution rates for biotite calculated from Si data in Table 3 and using initial- and final- BET SSA (BET), geometric SSA (Geometric), geometric edge SSA (EDGE) or mass (Mass) as the rate normalising term (10^{-12} $mol_{biotite}$ m^{-2} s^{-1})

Grain size (μm)	Normalising term—initial			
	BET	Geometric	EDGE	Mass
180–150	1.58	6.31	110.43	0.89
	1.43	5.70	99.70	0.81
105–90	1.30	4.77	62.84	0.86
75–63	1.25	3.26	59.46	1.15
53–20	1.64	6.39	64.75	2.37
	1.69	6.58	66.63	2.43
20–10	1.28	14.40	68.41	6.08
	1.30	14.59	69.29	6.16
Average	1.43	7.75	75.19	2.59
SD (%)	12	56	25	88
	Normalising term—final			
	BET	Geometric (constant *c* dimension, see Fig. 1)	EDGE	Mass
180–150	**1.56**	6.41	111.32	0.91
	1.09	5.78	100.44	0.82
105–90	1.05	4.83	63.31	0.87
75–63	1.02	3.33	60.12	1.17
53–20	1.37	6.68	66.26	2.48
	1.54	6.86	68.10	2.54
20–10	**1.55**	16.03	72.65	6.86
	2.03	16.21	73.50	6.93
Average	1.40	8.27	76.96	2.82
SD (%)	24	60	24	92

Where two values are given these are for replicate experiments. Pairs of data in bold are significantly different ($p \leqslant 0.05$).

of experiments using the same grain size fraction were statistically identical except for ($p \leqslant 0.05$) the 180–150 and 20–10 μm final BET SSA normalised biotite rates. The similarity in dissolution rate between pairs of the same-sized particles gives confidence that any difference in rates between grain sizes is not due to experimental uncertainty.

Anorthite initial- and final-BET normalised dissolution rates (Table 4) are about an order of magnitude lower than values of ca. 1×10^{-9} mol m^{-2} s^{-1} reported in the literature (e.g., Oelkers and Schott, 1995; Lütgge et al., 1999). The limiting step in feldspar dissolution differs between anorthite and the alkali feldspars because of the ratio of Al–O to Si–O bonds in the structure (Oelkers and Schott, 1995). Therefore dissolution rates of anorthite are highly sensitive to the purity of the crystals. The anorthite dissolved in this experiment was An92, the anorthite dissolved by Oelkers and Schott (1995) An96 and by Lütgge et al. (1999) An98. Thus, the discrepancy between the anorthite BET normalised dissolution rates obtained in this study and those obtained by Oelkers and Schott (1995) and Lütgge et al. (1999) may be due to purity of the anorthite dissolved.

Relatively few biotite dissolution data are available for comparison in the literature. Acker and Bricker (1992) report rates of $2.9–6.4 \times 10^{-12}$ mol m^{-2} s^{-1}, Kalinowski and Schweda (1996) $1.6–5.0 \times 10^{-12}$ mol m^{-2} s^{-1} and Malmström and Banwart (1997) 2.8×10^{-11} mol m^{-2} s^{-1}. These are relatively similar to the rates reported here.

For each normalising term for anorthite and biotite, significant variation ($p \leqslant 0.05$) exists in the dissolution rates calculated across the range of grain sizes. This is the case for biotite even if the 180–150 and 20–10 μm final BET SSA normalised rates (i.e., rates from experiments which showed a significant difference between the replicates of the same grain size fraction) are omitted from the analysis. Thus, from a statistical perspective none of the normalisation terms used in the calculations that give rise to the dissolution rates in Tables 4 and 5 would be considered appropriate. However, it should be noted that this analysis does not take into account the uncertainty associated with the individual terms in Eq. (2).

Uncertainties associated with the terms in Eq. (2) are approximately ±1% for q, ±10% for [Si], ±1% for M and, ±10% for SSA. Uncertainties in the calculated dissolution rates equal the sum of the uncertainties of the terms in Eq. (2) and therefore uncertainty in dissolution rates normalised to SSA are ±22% and for rates normalised to mass ±12%. If error bars of these magnitudes are applied to the mean normalised dissolution rates reported in Tables 4 and 5 then for anorthite, normalisation to initial BET SSA and initial and final geometric SSA gives constant dissolution rates whilst for biotite only normalisation to initial BET SSA gives a constant dissolution rate across grain sizes. This result is consistent with the size of the standard deviations about the mean dissolution rate for the different normalising terms (Tables 4 and 5). The standard deviations indicate that for biotite, rates normalised to initial- and final-geometric edge SSA and final BET SSA form the next "least varied" rates after rates normalised to initial BET SSA.

Hodson (2002) dissolved different size fractions of the mineral fraction of the B horizon of a granitic podzol in batch experiments using pH 4, HCl. Quartz, plagioclase feldspar, alkali feldspar, chlorite, and biotite were present in the fractions. After taking into account differences in

mineralogy, Hodson showed that both the BET- and geometric- SSA normalised dissolution rate of the finest size fraction (53–2 μm) was significantly greater than those of the 2000–500, 500–250, and 250–53 μm fractions. He hypothesised that this result could be due to: (1) greater reactivity of smaller particles due to free energy effects, (2) an increase in the ratio of reactive to geometric and BET surface area with decreasing grain size or, (3) the presence of highly reactive minerals in the finest fraction that were undetected by X-ray diffraction due to their low concentration. The results from the current experiments favour the third explanation. Although the 20–10 μm final geometric SSA normalised rate for biotite and the 20–10 μm final BET SSA normalised rate for anorthite are significantly greater than for the other grain sizes, Hodson's (2002) first two hypotheses require both geometric- and BET SSA normalised rates to be significantly greater.

The increase in mass normalised dissolution rate with decreasing grain size for both anorthite and biotite is consistent with dissolution occurring over the mineral surface. For a given mass of particles, smaller grain sizes will yield more surface than larger particles and therefore more dissolution will occur per unit mass of particles.

3.3.1. Anorthite SSA normalised dissolution rates

Unlike the studies of Gautier et al. (2001) and Stillings and Brantley (1995) in this experiment final dissolution rates across grain sizes were compared rather than comparing the dissolution rate of a particular mineral powder as dissolution proceeded and surface area evolved. Lee et al. (1998) demonstrated that although dissolution can occur far more rapidly at etch pit sites on feldspar surfaces, in far from equilibrium conditions of the sort utilised in laboratory mineral dissolution experiments bulk dissolution rate is dominated by the dissolution of non-etched surface. This is because the surface area of the non-etched surface is far greater than that of the pit floors. Gautier et al. (2001) demonstrated the same for quartz. Lee et al. (1998) and Gautier et al. (2001) also proposed that the walls of etch pits are relatively unreactive. Following these lines of reasoning an appropriate dissolution rate normalising term that would give constant rates over time and across grain sizes would be one that scales to the non-etched surface or, given the small areal extent of etch pit floors, the entire surface of a grain excluding the unreactive etch pit walls. Initial and final geometric SSA do this as they are calculated assuming a smooth grain surface with no surface features. Initial BET SSA should also do this provided that grains are either free from surface features prior to dissolution or that any surface topography that is measurable as BET SSA is uniformly present at all grain sizes. For the anorthite dissolved here SEM observations indicate that the former was the case. It is interesting to note that on the basis of a comparison between rates derived using the data of Oelkers and Schott (1995) and interferometry measurements Lütgge et al. (1999) also concluded that using initial BET SSA for normalising dissolution rates "is, at least for the case of anorthite, a rather reasonable estimate of the reactive surface area." Despite including surface area associated with the unreactive walls of dissolution features normalisation to final BET SSA should also give constant dissolution rates across grain sizes provided that there is a uniform distribution of dissolution features (though as in Gautier et al. (2001) the rates would change over time as the proportionality between reactive and BET surface area changes as dissolution generates more unreactive BET surface area, i.e., the etch pit walls). However, in this experiment there was not a uniform distribution of such features. As well as etch pits being produced by dissolution, more linear dissolution cracks were observed to form in some grains (e.g. Fig. 2b). Point counting of SEM images obtained using a JEOL JSM 5300 running at an accelerating voltage of 20 kV indicates that the relative abundance of dissolution cracks decreases with decreasing grain size. Grains from the 20–10 μm size fraction are hardly cut by dissolution cracks at all (Fig. 3). By analogy with etch pits the dissolution cracks are interpreted to have formed by dissolution of planes of strain or some other planar instability within the mineral grains. Along these planes grains preferentially: (1) break when ground (thereby explaining the reduced frequency of the dissolution channels in the finer grain size fractions) and (2) dissolve (forming the dissolution cracks). The net result of the formation of the cracks is that final BET SSA normalised rates are smaller for the coarser fractions than the finer fractions due to the inclusion of a greater proportion of unreactive BET SSA (the crack walls) in the calculation.

It seems likely that the dissolution rates normalised to initial BET SSA and initial- and final- geometric SSA would remain constant over time like those of quartz determined by Gautier et al. (2001) rather than increasing like those of various plagioclases determined by Stillings and Brantley (1995). The anorthite dissolved here was near-end member anorthite from the albite–anorthite solid solution series; it dissolved through the formation of etch pits and cracks. This is essentially the same as the quartz of Gautier et al. (2001). The plagioclases that Stillings and Brantley (1995) dissolved were intermediate members of the albite–anorthite solid solution series and would have contained zones of differing composition and reactivities; as dissolution proceeded zones of different reactivities

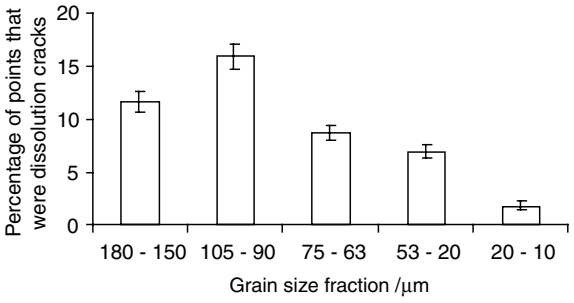

Fig. 3. Percentage of "hits" for dissolution cracks obtained by point counting SEM images of anorthite grains after dissolution. ca. 4500 randomly selected points were counted for each size fraction. Size fractions were imaged at a level of magnification so that 6–11 grains were in the field of view. Error bars, standard error.

would have been encountered by the floors and walls of deepening dissolution features.

In the field only current surface areas can be measured. These are analogous to the final surface areas measured in the laboratory. The results of this study suggest that in comparison studies final geometric SSA should be used to normalise laboratory determined dissolution rates and current geometric SSA for field rates.

3.3.2. Biotite SSA normalised dissolution rates

Although the biotite dissolved its surface remained smooth on the scale of SEM observations (e.g. Fig. 2c). This is consistent with various studies that suggest that dissolution of sheet silicates is concentrated at grain edges (Ross, 1969; Knuass and Wolery, 1989; Acker and Bricker, 1992; Turpault and Trotignon, 1994; Kalinowski and Schweda, 1996; Rufe and Hochella, 1999; Bosbach et al., 2000; Köhler et al., 2005). If dissolution only occurred at grain edges it would be expected that dissolution rates normalised to geometric edge SSA would show least variation. Whilst both initial and final geometric edge SSA are present in the second best group of normalising terms (Table 5) it is initial BET SSA normalised rates that show the least variation across grain sizes. Unless surface roughness (the ratio of BET to geometric surface area, Helgeson et al., 1984) varies randomly with both crystallographic orientation and grain size, BET SSA would only scale to biotite edge surface area if the ratio of grain dimensions remained constant across grain sizes. SEM observations indicate that this is not the case for the biotite size fractions dissolved in this experiment. If the 180–150 μm data are removed from the analysis then the standard deviations about the mean rate for the remaining size fractions become 6% and 8% for rates normalised to initial and final geometric edge SSA respectively (though statistically significant differences still exist between the rates of the different grain sizes); standard deviation for rates calculated using the other normalising terms remain essentially unchanged. Unfortunately there is no obvious reason to discount the 180–150 μm data. The solution chemistry data appear to be of the same quality as the data obtained for the other size fractions and there is no indication from SEM observations that the coarser grains might contain more fractures or cracks to generate additional unaccounted geometric edge SSA relative to the smaller grains. Turpault and Trotignon (1994) suggest that SEM observations to calculate geometric edge surface area may contain systematic underestimates of the magnitude of this term. It is not clear from their paper whether they would expect this error to be constant in absolute or percent terms. If percentage underestimation was constant with varying grain size then its contribution to the current discussion may be ignored but if the percentage underestimation was greater for coarser grains this might explain the larger edge normalised dissolution rates for the 180–150 μm fraction observed here (which result in the larger standard deviation). On the basis of SEM and AFM observations (e.g., Nonaka, 1984) a surface roughness of ca. 1 can be assigned to the basal surfaces of mica. It is then possible to recalculate edge SSA as the difference between BET SSA and a geometric calculation for basal SSA (Table 6). Percentage increase in calculated edge SSA is greatest for the coarsest grains. Thus, it is highly possible that the underestimate in edge SSA that Turpault and Trotignon (1994) propose is greater for coarser grains. However, the rates normalised to the new initial and final edge SSA are almost identical in value to the intial- and final-BET normalised rates; the rates still have a standard deviation of 17% for initial values and 25% for final values. Thus, it would appear that any errors in the calculation of edge surface area do not fully account for why the rates normalised to edge SSA show greater variation than those normalised to initial BET SSA.

One interpretation of the data is that some biotite dissolution must be occurring over basal surfaces as well as edge surfaces, though at a different rate. The ratio of edge to basal surface area is not constant across grain sizes resulting in variation in calculated dissolution rates. The ratios of edge to basal geometric SSA decrease from 1:3.7 in the 20–10 μm fraction to 1:16.6 in the 180–150 μm fraction. Following the method of Turpault and Trotignon (1994) Eq. (3) was solved using initial- and final-geometric SSA normalised rates, geometric edge SSA and geometric basal SSA (calculated as geometric SSA-geometric edge SSA) and a least squares fitting procedure.

$$R_{\mathrm{Si}} = r_{\mathrm{edge}} \cdot \mathrm{S}_{\mathrm{edge}} + r_{\mathrm{basal}} \cdot S_{\mathrm{basal}}, \tag{3}$$

where r_{edge} is the dissolution rate of edge surfaces of biotite ($\mathrm{mol_{biotite}\,m^{-2}\,s^{-1}}$); r_{basal} is the dissolution rate of basal surfaces of biotite ($\mathrm{mol_{biotite}\,m^{-2}\,s^{-1}}$); S_{edge} is the fraction of surface area due to edge surface; and S_{basal} is the fraction of surface area due to basal surfaces.

Table 6
Comparison of biotite edge SSA terms calculated either purely from geometric considerations (EDGE1) or a combination of BET SSA and geometric considerations (EDGE2) ($\mathrm{m^2\,g^{-1}}$)

Grain size (μm)	Initial edge surface area ($\mathrm{m^2\,g^{-1}}$)			Final edge surface area ($\mathrm{m^2\,g^{-1}}$)		
	EDGE1	EDGE2	% increase	EDGE1	EDGE2	% increase
180–150	0.008	0.430	5275	0.008	0.448	5500
	0.008	0.430	5275	0.008	0.616	7600
105–90	0.014	0.494	3429	0.014	0.665	4650
75–63	0.019	0.584	2974	0.020	0.816	3980
53–20	0.037	1.109	2897	0.037	1.470	3873
	0.037	1.109	2897	0.037	1.318	3462
20–10	0.089	4.403	4847	0.094	4.100	4262
	0.089	4.403	4847	0.094	3.085	3182

Where two values are given these are for replicate experiments. EDGE1 calculated from the surface area occupied by surfaces *ac* and *bc* (see Fig. 1) using the formula EDGE1 = 2(*ac* + *bc*)/particle mass; EDGE2 calculated by subtracted the geometric SSA due to surfaces *ab* (see Fig. 1) from BET SSA using the formula EDGE2 = BET SSA − (2 *ab*/particle mass); % increase is the increase in Edge SSA when it is calculated as EDGE2 as opposed to EDGE1, i.e., % increase = 100 × (EDGE2 − EDGE1)/EDGE1.

For initial SSA values, dissolution rates for edge and basal surfaces of the biotite were 64.07 and 0.91×10^{-12} $mol_{biotite}\ m^{-2}\ s^{-1}$. For final SSA values, dissolution rates for edge and basal surfaces of the biotite were 70.30 and 0.53×10^{-12} $mol_{biotite}\ m^{-2}\ s^{-1}$. This gives ratios of edge to basal dissolution rates of 71 for the initial values and 132 for the final values which lie within the range of 30 and 300 suggested by Turpault and Trotignon (1994). The lower variation of rates normalised to initial BET SSA than final BET and initial- and final-geometric SSA indicates that for this experiment initial BET SSA best integrates the different rates and surface areas of the basal and edge surfaces.

If an experiment similar to that of Gautier et al. (2001) was performed for biotite the steady state rates determined here would most likely vary with time. The ratio of edge to basal surface area would only remain constant if the length, width, and thickness dimensions of the biotite grains all changed by the same factor as dissolution proceeded. Given the relative dissolution rates of these different surfaces this is unlikely to happen. Thus, the steady state rates determined in the current experiment would more properly be termed pseudo-steady state rates. They may only appear constant because they change at a rate that is undetectable over the time period of measurement used in this experiment. This supposition is consistent with the work of Köhler et al. (2005) who, on the basis of their own experiments on illite, and reported experiments on illite, montmorillonite, kaolinite, and muscovite, concluded that sheet silicates dissolve preferentially at their edges and that during dissolution the amount of reactive edge sites decrease so that these minerals can never attain a steady state dissolution rate.

These results suggest that extrapolation of laboratory derived biotite dissolution rates to the field will always be problematic. As suggested by Köhler et al. (2005), calculations must take into account the evolution of the edge to basal area ratio with time. Alternatively, it may be the case that after a certain amount of dissolution, change in the edge to basal surface area ratio is so minimal compared to the uncertainties associated with mineral dissolution calculations that the pseudo-steady state rates measured in the laboratory may be approximated to true steady state rates. In which case, this study suggests that final-(laboratory) and current-(field) BET or geometric edge SSA should be used for laboratory-field comparisons. Given the problems producing monomineralic separates from soils in order to obtain BET SSA measurements it is recommended that geometric edge SSA is used.

4. Conclusions

If it is accepted that normalised dissolution rates should be constant across grain sizes then for the purposes of laboratory dissolution experiments initial BET, initial geometric or final geometric SSA would appear to be suitable normalising terms for dissolution rates determined on the previously unweathered mineral separates of anorthite dissolved here. The different size fractions had different densities of highly reactive surface area which was manifest as a higher density of deep cracks running across the coarser grains after dissolution. This should not have significantly influenced bulk element release from the anorthite due to the relatively small area of these sites. However, it led to the generation of more unreactive BET surface area in the coarser grains and consequently final BET SSA normalised rates were lower for the coarser grains.

For biotite, normalisation to initial BET surface area resulted in the least varied dissolution rates across grain sizes. Although biotite dissolves from its edges some dissolution does occur over the basal surfaces. For the different size fractions dissolved here the ratio of edge to basal surface varied with grain size explaining why dissolution rates normalised to edge surface area did not give the least variation across grain sizes. Initial BET SSA best integrated the different dissolution rates and areas of the edge and basal surfaces of biotite.

Steady state dissolution rates can only be achieved if dissolution neither generates or destroys reactive surface area. These experiments indicate that this should be the case for anorthite where dissolution proceeds via the formation of dissolution features with negligible floor area and unreactive walls but not for biotite where the ratio of edge to basal surfaces, which dissolve at different rates, will change as dissolution proceeds. However, after sufficient dissolution a stage may be reached where the rate of change of dissolution rate of biotite (and other sheet silicates) is sufficiently small that, within the context of uncertainties associated with calculated mineral dissolution rates, the pseudo-steady state rates may be approximated to a true steady state rate.

To compare laboratory and field dissolution rates final laboratory and current field SSA or mass must be used as normalising terms. It is impractical to produce monomineralic separates from soils for BET analysis. Therefore, these results indicate that final geometric SSA should be used for anorthite- and final geometric edge SSA for biotite- laboratory determined dissolution rate normalisation.

Acknowledgments

This work was carried out on equipment purchased by a Royal Society New Lecturers grant. Discussions with colleagues including Sue Brantley, Jiwchar Ganor, Martin Lee, Eric Oelkers, Ian Parsons, Susan Stipp, Domenik Wolff-Boenisch, and Art White helped clarify my thoughts on the vexed issue of reactive surface area and proxies for it. Chris Jones at the Natural History Museum (London, UK) where the author is a scientific associate is thanked for access to the Philips XL-30. Justine Ponzi is thanked for assistance with the JEOL JSM 5300 in Reading. Eric Oelkers, Andreas Lüttge, Felix Brandt, Domenik Wolff-Boenisch, Rolf Arvidson, Suvasis Dixit, and an anonymous reviewer are thanked for helpful comments on the manuscript.

Associate editor: Eric H. Oelkers

Appendix A

Anorthite solution composition over the duration of the experiment (μg L^{-1})

Size fraction (μm)		Elapsed time (h)																							
		24	48	312	384	696	744	840	984	1080	1488	1656	1872	2016	2184	2328	2496	3024	3168	3576	3840	4056	4872	5376	6360
	Concentration (μg L^{-1})																								
180–150	Al	3590	4008	5123	4106	4892	4410	4348	5284	4964	5266	3532	4151	4532	4999	4659	4340	2737	2600	2474	3378	3385	2738	2471	3322
	Ca	6477	5293	3971	3238	3839	3467	3495	3937	3724	3858	3157	3062	3375	3648	3485	3202	2245	2146	2098	2839	2870	1972	1809	2405
	Si	3425	3873	5135	4018	4816	4373	3949	4242	4216	4184	2923	3738	4922	5345	5126	4381	2843	2941	2823	3826	3908	2777	2460	3398
	pH																				3.4	3.4	3.5	3.4	3.5
180–150	Al	3597	3810	4042	4584	4652	4453	4577	5294	5378	5556	3320	3600	4558	4056	4193	4131	3270	3022	2144	2174	2389	2907	2605	3273
	Ca	6797	5246	3039	3397	3448	3407	3535	3980	4151	4201	2722	2598	4089	3518	3089	3150	2612	2657	1911	2035	2094	2025	1932	2373
	Si	3508	3613	3883	4334	4478	4417	4225	4217	4655	4492	2693	3113	4944	4515	4488	4298	3537	3637	2462	2548	2641	2820	2706	3317
	pH																				3.4	3.4	3.4	3.5	3.5
105–90	Al	4162	5582	4801	4193	4964	4714	4590	5778	6069	5029	3468	4199	4023	3831	3992	4425	3055	3021	2705	2444	2677	3410	1129	3266
	Ca	6072	5985	3415	3001	3606	3420	3671	4250	4386	3557	2719	3004	3162	2979	2945	3080	2724	2526	2396	2159	2347	2045	575	2312
	Si	3961	5452	4469	3926	4834	4525	4202	4569	4797	3853	2747	3807	4487	4380	4387	4672	3717	3503	3202	2960	3043	2835		3284
	pH																				3.5	3.5	3.5	3.5	3.5
105–90	Al	8001	3826	3765	4282	3215	3355	4255	6112	6123	5728	4025	4466	4669	4323	4930	4209	2904	2963	2210	1991	2164	3394	2661	3530
	Ca	9322	4755	3353	3321	2924	2930	3155	4674	4447	4318	2974	3290	3373	3178	3654	3120	2776	2861	2048	1810	1917	2564	1970	2616
	Si	7980	3686	3594	4106	3070	3199	3818	4778	4942	4501	3077	4097	5045	4717	5384	4470	3568	3599	2662	2381	2391	3566	2759	3607
	pH																				3.4	3.4	3.7	3.4	3.5
75–63	Al	6898	4476	4470	4347	3603	3736	4314	5091	4968	4655	4476	3531	3638	4627	3951	3938	2730	3026	2673	2538	2777	2916	2955	3746
	Ca	7909	4630	3394	3302	2774	2950	3298	3653	3607	3424	3314	2616	3729	3475	3464	3200	2612	2870	2733	2338	2540	2392	2138	2892
	Si	6753	4196	4300	3936	3302	3345	3672	3745	3802	3582	3469	3273	4015	4951	4208	4268	3348	3683	3331	3101	3102	3044	3066	3825
	pH																				3.6	3.6	3.5	3.7	3.5
75–63	Al	4963	4126	4719	4773	3665	3982	4446	5228	7513	6191	4476	3693	4806	5025	5416	13	3248	2931	2857	2613	2607	3003	2643	3309
	Ca	6731	4590	3557	3722	2788	2940	3405	3878	4901	4481	3381	2876	4243	4333	4406	644	2844	2859	2642	2305	2400	2136	1904	2355
	Si	4237	3619	4255	4629	3294	3572	3951	3929	4348	4830	3360	3378	5285	5393	5494	25	3813	3579	3476	3082	3173	3082	2773	3422
	pH																				3.6	3.6	3.5	3.7	3.6
53–20	Al	5699	5653	5516	5534	5000	—	5934	6687	6214	5756	5393	4721	4721	4852	4985	4313	3055	2938	2752	2699	2674	3287	3110	4337
	Ca	5790	4833	4150	4350	3797	—	4640	4969	4654	4492	3973	3626	3642	3758	3568	3470	3243	2828	2604	2432	2472	2355	2218	3033
	Si	5065	5091	5147	5196	4671	—	5087	5057	4759	4371	4001	4264	5262	5361	5281	4700	3616	3625	3371	3289	3209	3311	3165	4193
	pH																				3.6	3.6	3.6	3.7	3.6
53–20	Al	5330	5716	5373	5295	5035	4760	5722	6246	5976	5108	4937	4071	4378	4553	4461	3769	3536	3702	3407	3106	3423	3063	2691	3485
	Ca	4977	4670	4117	4206	3585	3728	4361	4976	4637	3978	3927	3007	3193	3484	3221	2905	2747	2848	2756	2278	2552	2138	1890	2649
	Si	4756	5134	4926	4856	4335	4382	4845	4712	4517	3802	3699	3687	4821	5050	4840	4163	3735	3667	3515	3225	3165	2937	2685	3533
	pH																				3.6	3.6	3.7	3.6	3.6
20–10	Al	5834	5180	5311	5405	4386	4207	4199	—	—	—	—	3698	3484	3436	2978	2953	3092	2724	3574					
	Ca	5525	5286	4627	4459	3468	3027	3011	—	—	—	—	2916	2940	2770	2422	2421	2248	1949	2544					
	Si	5748	4569	6921	4754	3688	3431	3821	—	—	—	—	4103	3767	3805	3405	3407	3233	2786	3685					
	pH															3.6	3.4	3.4	3.5	3.4					

Data from each replicate experiment are given.

Appendix B

Biotite solution composition over the duration of the experiment (μg L^{-1})

Size fraction (μm)		Elapsed time (h)																				
		0	24	48	120	192	480	648	816	984	1992	1320	1728	1152	2496	2856	3240	3480	4008	4320	4728	4992
	Concentration (μg L^{-1})																					
180–150	Al	857	686	543	379	398	367	326	324	300	275	310	268	291	313	280	286	271	271	272	275	314
	Fe	2273	2100	2029	2032	1752	1304	954	775	662	622	828	703	690	685	657	580	587	524	516	626	704
	K	3501	2781	2354	1379	1066	793	524	613	523	469	641	445	401	397	200	413	385	417	382	421	438
	Mg	2464	1959	1692	960	729	533	437	470	429	406	468	406	404	428	381	396	381	384	373	414	461
	Si	1694	1646	1504	1261	1108	972	842	786	785	710	754	723	737	739	630	689	651	680	671	670	802
	pH																	3.2	3.2	3.1	3.2	3.1
180–150	Al	717	630	566	353	491	380	298	316	337	275	245	244	273	236	263	300	223	251	265	249	246
	Fe	1806	2082	1151	1515	2068	1439	894	859	702	725	671	598	624	588	616	647	499	574	629	581	585
	K	3064	2665	2277	1127	1461	921	339	794	649	545	484	384	394	396	300	415	273	422	425	413	402
	Mg	2042	1873	1661	843	877	593	408	485	490	430	391	367	384	350	366	424	328	368	375	400	375
	Si	1374	1490	1525	1098	1490	1032	778	772	827	715	611	618	620	574	584	700	545	650	659	625	652
	pH																	3.1	3.2	3.1	3.1	3.2
105–90	Al	614	458	313	254	260	271	276	279	262	281	272	207	216	227	259	224	218	229	221	244	270
	Fe	2239	1874	1735	1445	1298	1407	1142	950	677	741	734	619	578	554	457	552	546	439	457	558	615
	K	3823	3010	2175	1129	798	577	480	625	504	549	524	361	296	210	148	373	305	355	334	359	393
	Mg	2371	1971	1664	986	811	589	464	469	421	433	436	346	315	325	337	342	331	315	315	363	385
	Si	1401	1188	1007	825	756	747	711	637	604	650	770	584	564	524	552	548	516	540	591	560	661
	pH																	3.1	3.2	3.1	3.1	3.1
75–63	Al	445	339	332	433	373	398	358	319	280	249	255	238	252	261	228	228	218	230	206	202	228
	Fe	1324	1219	1578	2426	1944	1920	1267	970	665	730	694	623	623	602	560	448	475	544	513	491	516
	K	3517	2523	2213	1604	1050	967	545	723	639	410	443	407	345	376	123	301	278	376	281	336	338
	Mg	2466	2036	1892	1333	862	620	502	494	441	3293	400	361	358	359	321	329	312	325	298	299	345
	Si	1228	1119	1076	1138	990	1012	897	762	669	621	688	649	648	610	537	561	523	585	541	545	604
	pH																	3.1	33.1	3.1	3.2	3.1
53–20	Al	586	553	639	591	624	413	414	360	359	307	367	300	348	378	318	343	616	297	325	279	321
	Fe	2183	2646	3420	2898	2242	1120	1035	729	760	802	968	708	821	795	647	657	584	607	601	708	727
	K	3382	2806	2637	1747	1378	606	509	661	630	430	577	446	549	640	302	446	356	483	428	488	443
	Mg	2718	2263	1978	928	1007	585	559	532	526	464	538	438	476	504	429	463	371	396	431	452	474
	Si	1483	1601	1786	1475	1815	992	1023	857	853	765	949	818	877	858	716	809	624	688	809	716	790
	pH																	3.1	3.1	3.2	3.2	3.1
53–20	Al	555	465	440	385	367	295	276	281	246	251	251	240	252	269	260	238	228	250	245	223	268
	Fe	2081	2369	2586	2226	1486	948	753	781	581	584	591	591	590	447	522	509	521	465	572	556	618
	K	3030	2673	2406	1400	846	584	328	548	415	409	429	385	333	285	147	331	322	348	370	416	400
	Mg	2216	1998	1670	745	550	441	383	421	368	370	375	363	355	348	341	348	331	339	341	406	398
	Si	1257	1454	1466	1134	949	795	694	715	600	604	661	629	640	588	561	567	538	585	618	570	671
	pH																	3.1	3.1	3.2	3.2	3.1

(*continued on next page*)

Appendix B (*continued*)

Size fraction (μm)		Elapsed time (h)																		
		0	24	48	120	192	480	648	816	984	1992	1320	1728	1152	2496	2856	3240	3480	4008	4320	4728	4992
20–10	Al	674	623	580	380	501	307	290	271	276	290	282	288	300	294	271	263	245	236	230	219	237
	Fe	4271	4225	3781	1681	1432	801	644	537	669	623	725	654	645	478	545	531	542	466	532	492	535
	K	1788	1654	1546	780	760	401	158	427	394	342	399	404	330	301	169	354	293	371	304	369	348
	Mg	1824	1286	993	601	702	413	365	414	403	416	429	413	399	394	362	378	354	340	323	368	355
	Si	1548	1449	1373	921	1281	677	594	570	595	648	679	736	733	671	617	639	581	570	574	550	596
	pH																	3.2	3.1	3.2	3.2	3.1
20–10	Al	662	574	569	417	364	328	309	354	310	280	280	291	303	315	260	245	266	246	243	213	268
	Fe	4066	3917	3717	1779	1147	801	720	559	839	691	628	636	643	664	578	501	558	535	477	505	572
	K	1669	1577	1542	899	615	379	258	460	532	430	467	469	363	282	136	286	275	368	319	346	351
	Mg	1891	1255	996	648	547	448	408	430	435	419	427	412	398	404	341	343	358	337	335	350	376
	Si	1575	1398	1337	973	822	746	686	668	635	666	736	730	720	672	586	574	599	616	584	554	649
	pH																	3.1	3.1	3.2	3.1	3.2

Data from each replicate experiment are given.

References

Acker, J.G., Bricker, O.P., 1992. The influence of pH on biotite dissolution and alteration kinetics at low temperature. *Geochim. Cosmochim. Acta* **56**, 3073–3092.

Arvidson, R.S., Beig, M.S., Lüttge, A., 2004. Single-crystal plagioclase feldspar dissolution rates measured by vertical scanning interferometry. *Am. Mineral.* **89**, 51–56.

Berner, R.A., 1995. Chemical weathering and its effect on atmospheric CO_2 and climate. In: White, A.F., Brantley, S.L. (Eds.) *Rev. Mineral.* vol. 31, Mineral Soc. Am., Washington, DC, USA.

Berner, R.A., Sjoberg, E.L., Velbel, M.A., Krom, M.D., 1980. Dissolution of pyroxene and amphibole during weathering. *Science* **207**, 1205–1206.

Bosbach, D., Charlet, L., Bicknore, B., Hochella, M.F., 2000. The dissolution of hectorite: in situ, real-time observations using atomic force microscopy. *Am. Miner.* **85**, 1209–1216.

Brantley, S.L., 2004. Reaction kinetics of primary rock-forming minerals under ambient conditions. In: Drever, J.I. (Ed.), *Treatise on Geochemistry 5: Surface and Groundwater, Weathering and Soils.* pp. 73–117.

Brantley, S.L., Crane, S.R., Crerar, D.A., Hellmann, R., Stallard, R., 1986. Dissolution at dislocation etch pits in quartz. *Geochim. Cosmochim. Acta* **50**, 2349–2361.

Brunauer, S., Emmett, P.H., Teller, E., 1938. Adsorption of gases in multimolecular layers. *J. Am. Chem. Soc.* **60**, 309–319.

Deer, W.A., Howie, R.A., Zussman, J., 1992. *An Introduction to the Rock Forming Minerals*. Longman Scientific & Technical, London, p. 696.

Fenter, P., Park, C., Cheng, L., Zhang, Z., Krekeler, M.P.S., Sturchio, N.C., 2003. Orthoclase dissolution kinetics probed by in situ X-ray reflectivity: effects of temperature, pH and crystal orientation. *Geochim. Cosmochim. Acta* **67**, 197–211.

Gautier, J.-M., Oelkers, E.H., Schott, J., 2001. Are quartz dissolution rates proportional to B.E.T. surface area? *Geochim. Cosmochim. Acta* **65**, 1059–1070.

Grandstaff, D.E., 1978. Changes in surface area and morphology and the mechanism of forsterite dissolution. *Geochim. Cosmochim. Acta* **42**, 1899–1901.

Gratz, A.J., Bird, P., Quiro, G.B., 1990. Dissolution of quartz in aqueous basic solution, 106–236 °C: surface kinetics of ''perfect''-crystallographic faces. *Geochim. Cosmochim. Acta* **54**, 2911–2922.

Gregg, S.J., Sing, K.S., 1982. *Adsorption, Surface Area and Porosity*. Academic Press, London, UK.

Helgeson, H.C., Murphy, W.M., Aagaard, P., 1984. Thermodynamic and kinetic constraints on reaction rates among minerals and aqueous solutions. II. Rate constants, effective surface area and the hydrolysis of feldspar. *Geochim. Cosmochim. Acta* **48**, 2405–2432.

Hodson, M.E., 2002. Variation in element release rate from different mineral size fractions from the B horizon of a granitic podzol. *Chem. Geol.* **190**, 91–112.

Holdren, G.R., Speyer, P.M., 1985. Reaction rate–surface area relationships during early stages of weathering. I. Initial observations. *Geochim. Cosmochim. Acta* **49**, 675–681.

Holdren, G.R., Speyer, P.M., 1987. Reaction rate–surface area relationships during early stages of weathering. II. Data on eight additional feldspars. *Geochim. Cosmochim. Acta* **51**, 2311–2318.

Hu, X.M., Grossie, D.A., Higgins, S.R., 2005. Growth and dissolution kinetics at the dolomite–water interface: an in situ scanning probe microscopy study. *Am. Miner.* **90**, 963–968.

Kalinowski, B.E., Schweda, P., 1996. Kinetics of muscovite, phlogopite, and biotite dissolution and alteration at pH 1–4, room temperature. *Geochim. Cosmochim. Acta* **60**, 367–385.

Knuass, K.G., Wolery, T.J., 1989. Muscovite dissolution kinetics as a function of pH and time at 70 °C. *Geochim. Cosmochim. Acta* **53**, 1493–1501.

Köhler, S.J., Bosbach, D., Oelkers, E.H., 2005. Do clay mineral dissolution rates reach steady state? *Geochim. Cosmochim. Acta* **69**, 1997–2006.

Lee, M.R., Parsons, I., 1995. Microtextural controls of weathering of perthitic alkali feldspars. *Geochim. Cosmochim. Acta* **59**, 4465–4488.

Lee, M.R., Hodson, M.E., Parsons, I., 1998. The role of intragranular microtextures and microstructures in chemical and mechanical weathering: direct comparisons of experimentally and naturally weathered alkali feldspars. *Geochim. Cosmochim. Acta* **62**, 2771–2788.

Lütgge, A., Bolton, E.W., Lasaga, A.C., 1999. An interferometric study of the dissolution kinetics of anorthite: the role of reactive surface area. *Am. J. Sci.* **299**, 652–678.

Malmström, M., Banwart, S., 1997. Biotite dissolution at 25 °C: the pH dependence of dissolution rate and stoichiometry. *Geochim. Cosmochim. Acta* **61**, 2779–2799.

Marschner, H., 1995. *Mineral Nutrition of Higher Plants*. Academic Press, London, UK.

Nilsson, J., Grennfelt, P., 1988. *Critical Loads for Sulphur and Nitrogen*. Report from a workshop held at Skokloster, Sweden. March 1988. Nordic Council of Ministers.

Nonaka, A., 1984. Surface–area estimation from the adsorption–isotherm gradient at the linear portion by benzene and toluene vapors on mica and aluminium foil samples. *J. Colloid Interf. Sci.* **99**, 335–340.

Oelkers, E.H., 2001. General kinetic description of multioxide silicate mineral and glass dissolution. *Geochim. Cosmochim. Acta* **65**, 3703–3719.

Oelkers, E.H., Schott, J., 1995. Experimental study of anorthite dissolution and the relative mechanism of feldspar hydrolysis. *Geochim. Cosmochim. Acta* **59**, 5039–5053.

Oelkers, E.H., Schott, J., Devidal, J.-L., 1994. The effect of aluminium, pH, and chemical affinity on the rates of aluminosilicate dissolution reactions. *Geochim. Cosmochim. Acta* **58**, 2011–2024.

Parkhurst, D.L., Appelo, C.A.J., 1999. User's guide to PHREEQC (Version 2)—A Computer Program for Speciation, Batch-Reaction, One-Dimensional Transport, and Inverse Geochemical Calculations: U.S. Geological Survey Water-Resources Investigations Report 99-4259, p. 310.

Ross, G.J., 1969. Acid dissolution of chlorites: release of magnesium, iron and aluminium and mode of acid attack. *Clays Clay Mins.* **17**, 347–354.

Rufe, E., Hochella, M.F., 1999. Quantitative assessment of reactive surface area of phlogopite during acid dissolution. *Science* **285**, 874–876.

SPSS, 2003. SigmaStat 3.0 for Windows. SPSS Science SoftwareGmb. Erkrath, Germany.

Stillings, L.L., Brantley, S.L., 1995. Feldspar dissolution at 25 °C and pH 3: reaction stoichiometry and the effect of cations. *Geochim. Cosmochim. Acta* **59**, 1483–1496.

Turpault, M.-P., Trotignon, L., 1994. The dissolution of biotite single crystals in dilute HNO_3 at 24 °C: evidence of an anisotropic corrosion process of micas in acidic solutions. *Geochim. Cosmochim. Acta* **58**, 2761–2775.

Vinson, M.D., Lüttge, A., 2005. Multiple length-scale kinetics: an integrated study of calcite dissolution rates and strontium inhibition. *Am. J. Sci.* **305**, 119–146.

White, A.F., 2004. Natural weathering rates of silicate minerals. In: J.I. Drever, (Ed.), *Treatise on Geochemistry 5: Surface and Groundwater, Weathering and Soils*. pp. 133–168.

White, A.F., Brantley, S.L., 1995. Chemical weathering of silicate minerals. *Rev Mineral*. vol. 31. Mineral Soc. Am., Washington, DC, USA, pp. 1–22.

Wilson, M.J., 1975. Chemical weathering of some primary rock forming minerals. *Soil Sci.* **119**, 349–355.

Wolff-Boenisch, D., Gislason, S.R., Oelkers, E.H., Putnis, C.V., 2004. The dissolution rates of natural glasses as a function of their composition at pH 4 and 10.6, and temperatures from 25 to 74 °C. *Geochim. Cosmochim. Acta* **68**, 4843–4858.

Zhang, H., Bloom, P.R., Nater, E.A., 1993. Change in surface area and dissolution rates during hornblende dissolution at pH 4.0. *Geochim. Cosmochim. Acta* **57**, 1681–1689.